GEOLOGY | THE GEOLOGICAL SOCIETY OF AMERICA®

https://doi.org/10.1130/G45898.1

Manuscript received 6 December 2018
Revised manuscript received 18 February 2019
Manuscript accepted 25 February 2019

Published online 21 March 2019

A supervolcano and its sidekicks: A 100 ka eruptive chronology of the Fish Canyon Tuff and associated units of the La Garita magmatic system, Colorado, USA

Leah E. Morgan, Samuel A. Johnstone, Amy K. Gilmer, Michael A. Cosca, and Ren A. Thompson
U.S. Geological Survey, Denver Federal Center, Denver, Colorado 80225, USA

ABSTRACT

Establishing temporal constraints on major volcanic eruptions is limited by the precision of existing geochronometers. Prior work on the La Garita caldera (Colorado, USA), created by the eruption of the Fish Canyon Tuff, failed to resolve temporal differences between pre-, syn-, and post-collapse eruptive units. Here, we report $^{40}Ar/^{39}Ar$ geochronologic data supporting a ~100 ka eruptive history of the La Garita caldera, and resolving the timing of the pre-caldera Pagosa Peak Dacite, syn-caldera Fish Canyon Tuff, and post-caldera dacite of Nutras Creek. Minimizing uncertainty in neutron fluence by rotating samples during irradiation and employing Bayesian statistical interpretation of analytical data enables resolution of the ~60 ka pre-caldera eruptive history and a hiatus of 0–20 ka prior to the eruption of post-caldera lavas. The improved precision demonstrated using these methods provides previously unresolvable temporal constraints on physical processes in the La Garita magmatic system and underscores the potential of unraveling other closely spaced events in geologic time.

INTRODUCTION

To understand cause-and-effect relationships, geologic processes, eruptive histories, and evolutionary events in Earth history, we must resolve the timing of closely spaced events. Volcanic units, whether they are sampled in proximal locations or as distal tephra units in a sedimentary record, are often used to understand these events, and they are commonly indistinguishable from their nearest neighbors. One of the most studied eruptions on Earth is the Fish Canyon Tuff (Colorado, United States), but it has not previously been resolved from its pre- and post-caldera eruptions. Here, we temporally resolve pre-, syn-, and post-caldera events in the Southern Rocky Mountain volcanic field to track magmatic cycles and understand the physical processes active in magmatic systems.

The Oligocene La Garita caldera and associated Fish Canyon Tuff (ca. 28 Ma) in southern Colorado record one of the largest volcanic eruptions known on Earth. Erupted ignimbrite volumes are estimated at >5000 km^3, and the eroded caldera (area >2600 km^2) contains pre- and post-caldera deposits of Fish Canyon magma interpreted as nearly contemporaneous eruptive products, bracketing the La Garita structural collapse (Lipman et al., 1997; Lipman, 2006; Bachmann et al., 2007). The eruptive phases of the La Garita system correspond to three lithostratigraphic map units (Fig. 1) of Lipman (2006): (1) Pagosa Peak Dacite (PPD)—pre-collapse "blob-and-ash" and massive lava-like deposits preserved adjacent to the southern caldera margin; (2) Fish Canyon Tuff (FCT)—intracaldera and outflow ignimbrite; and (3) dacite of Nutras Creek (NCD)—massive to flow-layered lava and breccia preserved in a small area on the north flank of the La Garita resurgent block. Estimated eruptive volumes for the pre-, syn- and post-collapse deposits are 200 km^3, >5000 km^3, and <1 km^3, respectively, (Lipman et al., 1997; Bachmann et al., 2000; Lipman, 2006). All three units are petrographically and chemically indistinguishable crystal-rich dacites.

Sanidine from the FCT eruption is a widely used neutron fluence monitor for $^{40}Ar/^{39}Ar$ geochronology, and the "absolute" age of Fish Canyon sanidine (FCs) from ignimbrite outflow deposits has been determined and revised numerous times (Cebula et al., 1986; Renne et al., 1998, 2010, 2011; Kuiper et al., 2008). Bachmann et al. (2007) determined statistically indistinguishable $^{40}Ar/^{39}Ar$ ages at the 2σ confidence interval for sanidine from PPD, FCT, and NCD (Fig. 2). Likewise, the >400 ka zircon crystallization history from Wotzlaw et al. (2013) tracks the thermal and chemical evolution of the La Garita magma chamber, but the youngest zircons from FCT and NCD are indistinguishable in age (PPD zircons were not analyzed) (Fig. 2).

In this study, we resolve the timing of pre-, syn- and post-caldera deposits of the La Garita system through $^{40}Ar/^{39}Ar$ geochronology by exploiting the rotation capabilities of the U.S. Geological Survey nuclear reactor. We utilize Bayesian analysis to measure the probability of age differences between samples with similar eruptive ages. For the first time, we can resolve an eruptive history that begins with the PPD ~60 ka prior to the eruption of FCT and likely continued for as much as 20 ka longer with the NCD.

SAMPLE ROTATION DURING IRRADIATION AND $^{40}Ar/^{39}Ar$ GEOCHRONOLOGY

While complications have been reported (Renne et al., 2012), sanidine typically records eruption ages of volcanic units, and it is present in most major units of the La Garita system. We performed $^{40}Ar/^{39}Ar$ geochronology on a total of nine samples from PPD, FCT, and NCD. Samples and neutron fluence monitors were irradiated in the same annular position of an aluminum irradiation disc (Fig. DR1 in the GSA Data Repository[1]); here, we used sanidine from the Fish Canyon Tuff (FCs-EK; Morgan et al., 2014) as a neutron fluence monitor, assuming an age of 28.201 Ma (Kuiper et al., 2008). Samples and monitors were rotated at 1 rpm throughout an 8 hr irradiation in the U.S. Geological Survey TRIGA reactor (Denver, Colorado) to minimize variations in the efficiency of reactor-produced argon generation. Rotation during irradiation aims to smooth neutron fluence gradients, allowing for the same *J* value (a function of neutron fluence; see Equations 1 and 2) to be applied to an annular ring of an irradiation disc (e.g. Schwarz and Trieloff, 2007). However, Rutte et al. (2015) showed that rotating the canister does

[1]GSA Data Repository item 2019173, details of analytical procedures and incremental heating experiments, Figures DR1–DR2, and Tables DR1–DR4, is available online at http://www.geosociety.org/datarepository/2019/, or on request from editing@geosociety.org.

CITATION: Morgan, L.E., et al., 2019, A supervolcano and its sidekicks: A 100 ka eruptive chronology of the Fish Canyon Tuff and associated units of the La Garita magmatic system, Colorado, USA: Geology, v. 47, p. 453–456, https://doi.org/10.1130/G45898.1

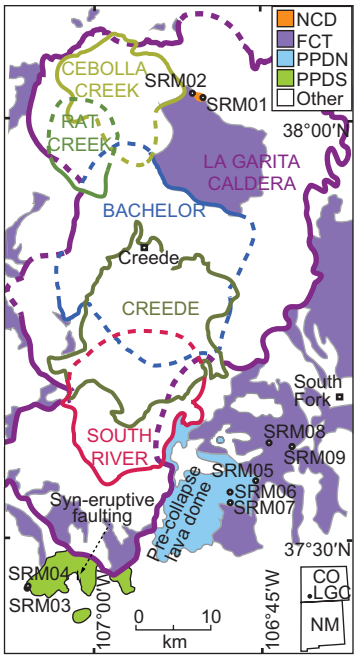

Figure 1. Simplified map showing caldera boundaries of central San Juan caldera cluster (southwestern Colorado, USA; modified from Lipman, 2006). Locations of analyzed samples are indicated, with northeastern and southwestern Pagosa Peak Dacite (PPD) samples separated. NCD—dacite of Nutras Creek; FCT—Fish Canyon Tuff; PPDN, PPDS—Pagosa Peak Dacite north and south, respectively; CO—Colorado; NM—New Mexico; LGC—La Garita caldera.

not guarantee equal fluence. Measurable fluence gradients can arise if the sample packet and rotation axis are not aligned parallel to the nuclear fuel elements. Here, ensuring parallel rotation yields a neutron fluence gradient of <0.1% across an 18.5 mm disc, based on *F*-values (the mean ratio of radiogenic to reactor-produced argon, $^{40}Ar^*/^{39}Ar_K$; after Dalrymple et al., 1981) for neutron fluence monitors placed at multiple positions around the disc.

Samples and standards were analyzed on a Thermo Scientific ARGUS VI mass spectrometer by multi-collection on four Faraday cups and one ion counter (for ^{36}Ar). Ages herein were calculated using an age of 28.201 Ma for the FCs neutron fluence monitor (Kuiper et al., 2008), decay constants (λ) of Min et al. (2000), and an atmospheric $^{40}Ar/^{36}Ar$ value from Lee et al. (2006). Analytical details, summary tables, and an argon isotopic data table can be found in the Data Repository (methods and Tables DR1–DR4) and in Morgan (2019).

Other studies have identified complex age spectra in the FCs monitor (Phillips and Matchan, 2013; Phillips et al., 2017; Jicha et al., 2016) that may indicate issues with pre-eruptive argon retention, recoil of ^{39}Ar,

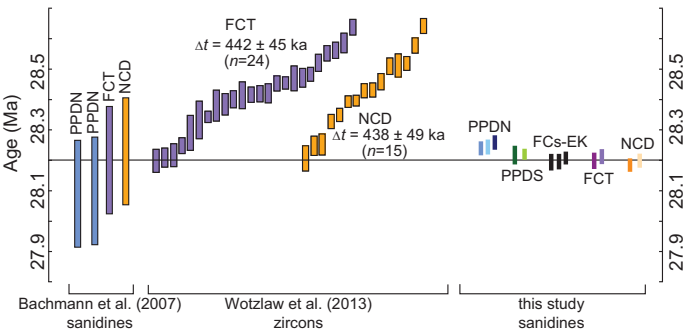

Figure 2. U-Pb zircon and $^{40}Ar/^{39}Ar$ sanidine geochronology of La Garita magmatic system (Colorado, USA), adapted from Wotzlaw et al. (2013). $^{40}Ar/^{39}Ar$ ages from Bachmann et al. (2007) were adjusted so that Fish Canyon Tuff (FCT) is 28.201 Ma, permitting direct comparison with results from this study. U-Pb zircon ages from Wotzlaw et al. (2013) record the duration of zircon crystallization in La Garita system. Previous results are shown with 2σ uncertainties. Interpreted eruption ages from this study, based on 95% credible interval (CI) from Bayesian modeling, have sufficient precision to highlight the range of eruption ages between units in La Garita system. Δ*t* —time difference; NCD—dacite of Nutras Creek; PPDN, PPDS, Pagosa Peak Dacite north and south, respectively; FCs-EK—sanidine from the Fish Canyon Tuff.

unresolved isobars, and/or isotopic fractionation during incremental laser heating. Similar complexities have also been identified in step-heating experiments on many samples considered here, but are not believed to have affected interpretations. See the Data Repository and Figure DR2 for further discussion and age spectra.

CALCULATING AGE DIFFERENCES

The *F*-value was assumed to reflect the time of an eruptive event (t_e), recognizing that past work has argued that this ratio may be influenced by other factors (e.g., Andersen et al., 2017; Phillips and Matchan, 2013; see the Data Repository for discussion):

$$t_e = \frac{1}{\lambda}\ln(1+JF), \quad (1)$$

where λ is the total decay constant for ^{40}K and *J* is a measure of the reactor production of ^{39}Ar from ^{39}K through comparison with a neutron fluence monitor:

$$J = \frac{e^{\lambda t_m}-1}{F_m}, \quad (2)$$

where t_m and F_m refer to the assumed age and measured *F*-value of the neutron fluence monitor, respectively.

Given our assumption that neutron fluence gradients are negligible (and thus *J* is constant) within an annular ring of an irradiation disc (an assumption we evaluate below), the expected difference in *F*-values between our unknowns and the FCs monitor representing the FCT is related to the ages of these samples as:

$$F_u - F_m = \frac{1}{J}\left(e^{\lambda t_u} - e^{\lambda t_m}\right). \quad (3)$$

Here, we refer to the age and *F*-value of unknowns as t_u and F_u, respectively. Expanding out *J* based on Equation 2, and expressing the timing of an unknown event as the sum of the age of our monitor and an offset, $t_u = t_m + \Delta t$, we obtain:

$$R - 1 = \frac{e^{\lambda t_m}\left(e^{\lambda \Delta t}-1\right)}{e^{\lambda t_m}-1}, \quad (4)$$

where *R* denotes the ratio of unknown to standard ratios, F_u / F_m. Given constant *J*, differences in mean age (e.g., non-zero values of Δ*t*) between the units in our sampled stratigraphy and the eruption of FCT will have values of *R* that are credibly different than 1. We can also rearrange this to directly compute the difference in age:

$$\Delta t = \frac{1}{\lambda}\ln\left(\frac{(R-1)\left(e^{\lambda t_m}-1\right)}{e^{\lambda t_m}}+1\right). \quad (5)$$

ASSESSING AGE DIFFERENCES WITH BAYESIAN ESTIMATION

If age differences are present, measurement variability from analytical uncertainty can result in overlap in the distributions of *F*-values between samples and monitors. Here, we are interested in whether there are credible differences between their mean ages, and hence mean *F*-values (Equation 5). Traditionally, weighted means have been used to represent the mean of a set of analyses, but they are sensitive to the inclusion or exclusion of outliers. Thus, we adopt a Bayesian alternative to the *t*-test modeled after Kruschke (2013), using a Markov chain Monte Carlo (MCMC) approach (Foreman-Mackey et al., 2013).

Individual crystals in a sample are characterized by an *F*-value ($F_{crystal}$) and an analytical uncertainty ($\sigma_{crystal}$). For each sample (~30 crystals per sample), we characterize the *posterior probability*, $p(F_{mean},\omega \mid \boldsymbol{F}_{crystal},\boldsymbol{\sigma}_{crystal})$, of the mean, F_{mean}, and an overdispersion term, ω, that accounts for variance not explained by analytical uncertainties (e.g., due to geologic phenomena). The posterior probability is proportional to the product of the *prior probability*, $p(F_{mean},\omega)$, and the *likelihood*, $p(\boldsymbol{F}_{crystal},\boldsymbol{\sigma}_{cystal} \mid F_{mean},\omega)$ of our

observations. We assign a Gaussian prior probability, $p(F_{mean}) = 8.944 \pm 0.042$ (1σ), defined by the mean and standard deviation of all $F_{crystal}$ values measured here to acknowledge previous work that found the geologic units studied here to be indistinguishable in age (Bachmann et al., 2007). We assign an uninformative prior expectation for the overdispersion term, $p(\omega) = 1$, as we have no existing expectations for the amount of overdispersion present. We follow Vermeesch (2018) and assume that the likelihood of any single crystal measurement is given by a normal distribution whose variance is the sum of that from analytical uncertainty and overdispersion: $N(F_{crystal} \mid F_{mean}, \sigma^2 = \sigma^2_{crystal} + \omega^2)$.

We run the MCMC model for 5000 iterations after a burn-in period of 1000 iterations with 200 "walkers" (each walker takes a guided step through the parameter space), resulting in 10^6 samples that characterize the posterior probability (we refer to the 10^6 numerical, randomized samples drawn for each geologic sample as MCMC samples). We summarize the credible intervals (CIs) for each sample's value of F_{mean} and ω^2 with the median and 95% interval of MCMC samples (Table DR1). Histograms of MCMC-sampled values of F_{mean}, which approximate the posterior probability, for each geologic sample are shown in Figures 3A and 3B.

We evaluate our assumption of constant J throughout the irradiation disk by comparing the posterior probabilities of the FCs monitors (FCs-EK separate; Fig. 3B). Substantial overlap of the CIs of the mean, F_{mean}, for all FCs monitors requires immeasurable differences in J (Equation 1). While there is also significant overlap in the CIs of samples SRM08 and SRM09 (also samples of the FCT; Fig. 3B), we preserve these as independent samples to document our ability to differentiate age differences of 0. Similarly, we do not group rock samples from the same geologic unit to evaluate the reproducibility of our results and allow for geologic variability. To incorporate observed variability and analytical uncertainty from all fluence monitors, we compute the posterior probability of F_m from a MCMC model where we pooled all single-crystal analyses for the fluence monitors (FCs-C1, FCs-C5, FCs-C9; see Fig. DR1) in evaluating the *likelihood* (FCs-EK pooled; Fig. 3B).

To determine the posterior probability of $R - 1$ (Equation 5), we difference every entry from the MCMC model of unknown sample means (F_u, sample SRM01-09) from the MCMC model of monitor means (F_m, FCs-EK pooled; e.g., Kruschke, 2013). The posterior probability of $R - 1$, specifically the probability that $R - 1$ values are >0 or <0, reflects our confidence in differences in the mean age of unknowns and the FCT. We also compute a modeled age difference (Equation 5; Table DR1) based on a mean assumed age of Fish Canyon sanidine (t_s) and the total decay constant (λ) (Min et al., 2000; Kuiper et al., 2008). While this doesn't account for uncertainty in t_m or λ, reported uncertainties in λ and t_m would propagate into Δt on the order of ~0.1% of Δt (assuming uncertainties in λ and t_m are uncorrelated).

For most samples analyzed here, the intersample variability in F_{mean} values is consistent with the measured analytical uncertainty (Table DR1). The additional variance (e.g., due to geologic dispersion), ω^2, is small with respect to the expected variance from analytical uncertainty (on average, the variance from analytical uncertainty is ~3× ω^2). This is consistent with MSWD values close to 1 (Table DR2). However, some samples do show signs of overdispersion. For sample SRM02, the variance from analytical uncertainty and ω^2 are comparable, and for samples SRM05 and SRM08 and the pooled FCs-EK, the median values of ω^2 are about one-half the variance expected from analytical uncertainty.

TIME SCALES OF ACTIVITY IN THE LA GARITA SYSTEM

The five PPD samples analyzed indicate a protracted, pulsed eruptive history of the PPD. These five samples are separated geographically (Fig. 1). Two samples (SRM03 and SRM04) are from the southwestern area of mapped PPD (here named PPD south, or PPDS), and three samples (SRM05, SRM06, and SRM07) are from the northeastern area of mapped PPD (here named PPD north, or PPDN). The CI bounds on differences in the mean age for these samples range from 13 ka younger to 78 ka older than FCT (Fig. 3). The two PPDS samples are not distinctly older than

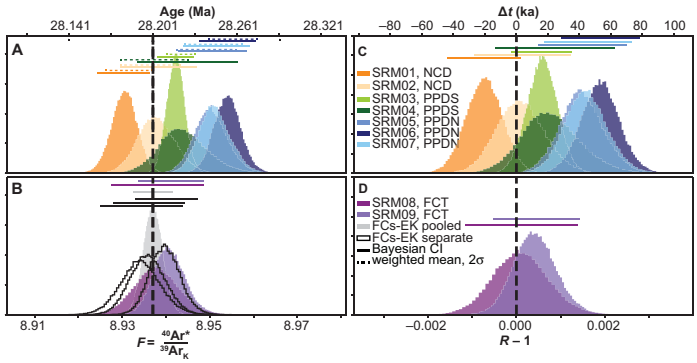

Figure 3. Results of Markov chain Monte Carlo (MCMC) characterization of argon geochronology of units from La Garita caldera (Colorado, USA). Bottom axes are derived from measured $^{40}Ar/^{39}Ar$ ratios (*F*-values [mean ratio of radiogenic to reactor-produced argon, $^{40}Ar^*/^{39}Ar_K$]), and top axes are calculated by asserting age of 28.201 for Fish Canyon Tuff (FCT) (Kuiper et al., 2008) for median of *F*-values from all sanidine from the Fish Canyon Tuff (FCs-EK) analyses. Distributions are histograms of 10^6 MCMC samples, divided into 100 evenly spaced bins and scaled so that the area under each curve integrates to 1. Credible intervals (CI) are shown as solid bars; preferred weighted mean ages (Table DR2 [see footnote 1]) are shown as dashed bars. A and B show *F*-values that best characterize units of FCT. C and D test the hypotheses that units pre- or post-date FCT (by time difference Δ*t*) by assessing the probability of differences in ages of units from FCs-EK (e.g., Equation 5 in text). *R* is the ratio of unknown to standard ratios, F_u / F_m (F_u—measured *F*-value of the neutron fluence monitor; F_m—*F*-value of unknowns). NCD—dacite of Nutras Creek; PPDS, PPDN—Pagosa Peak Dacite south and north, respectively.

FCT; the three PPDN samples define an interval from 15 to 78 ka prior to FCT. The PPDS samples are most likely younger than the PPDN samples. Prior studies inferred distinct eruptive sources for these areas, based on maximum thickness as distinct lobes, but were unable to discern relative ages from stratigraphic relations (Bachmann et al., 2000; Lipman, 2006).

The two FCT samples investigated here are from the lowermost and uppermost subunits of the FCT (respectively, units Tfc1 and Tfc6 of Lipman [2006]). The lowermost unit has long been used as a neutron fluence monitor for $^{40}Ar/^{39}Ar$ geochronology (Renne et al., 1998), but a recent sampling now in use as a standard (Morgan et al., 2014) was sourced from an intermediate subunit (unit Tfc5 of Lipman [2006]) and was shown to be indistinguishable from the lowermost unit in age. The CIs for all FCT samples and neutron fluence monitors overlap (Fig. 3). The eruption of NCD appears to have closely followed the caldera-forming FCT eruption, with both samples indistinguishable from FCT. The most likely age of sample SRM01 is younger than that of sample SRM02, but the range of credible ages for these samples overlaps. Because NCD overlies FCT, we conclude that NCD was concurrent with or postdated FCT by as much as ~20 ka (Fig. 3).

These new ages are consistent with the mapped geologic field relations of Lipman (2006) and with existing geochronology (Fig. 2). For example, (1) PPD everywhere underlies FCT along the southern caldera margin; (2) only the southern PPD is associated with faults interpreted as syn-collapse features; and (3) the single exposure of NCD is stratigraphically above FCT on the La Garita resurgent block of intracaldera FCT. However, the extended eruption time of the PPD and the migration of PPD eruption activity from north to south was not previously interpreted.

The time scales presented here for pre- and post-caldera formation in the La Garita system are broadly similar to those of relatively young, albeit smaller caldera systems, which display prolonged but episodic activity with periods of dormancy that alternate with periods of eruption (Druitt et al., 2002; Hildreth, 2004). As with the La Garita system, for example, the Long Valley magmatic system (California, USA) had extensive precursor activity for >1 Ma prior to the caldera-forming eruption of the Bishop Tuff at 0.76 Ma (e.g., Andersen et al., 2017; Mark et al., 2017). The last eruption

of Glass Mountain rhyolite (ca. 0.79 Ma) erupted ~30 ka before the Bishop Tuff (Metz and Mahood, 1985; Simon and Reid, 2005; Hildreth, 2004), while in the La Garita system, the eruption of the PPD began ~60 ka prior to the eruption of FCT.

SUMMARY

The combination of advances in sample rotation in the reactor and the application of Bayesian analysis allowed us to temporally discriminate between the PPD, FCT, and NCD, which were previously indistinguishable by either U-Pb in zircon or $^{40}Ar/^{39}Ar$ analyses of sanidine. For the ca. 28 Ma samples analyzed here, intervals as small as ~20 ka can be differentiated. Given that the PPD appears to have erupted intermittently over a protracted time span, the role of the PPD in triggering the FCT eruption (Bachmann et al., 2007) should be revisited.

Although discernible time differences such as these would vary in magnitude through Earth's history and with sample and data quality, the advances presented here may allow for determinations of small Δt values for a range of Earth science questions—including rates of evolutionary change, tectonic uplift, and other volcanic eruptive activity.

ACKNOWLEDGMENTS

We thank Pete Lipman for considering the geologic implications of our data and a helpful review of the manuscript, Brenhin Keller for advice on Bayesian modeling, Daniel Rutte for advice with sample rotation during irradiation, and Brett Davidheiser-Kroll for assistance with fieldwork. We thank Tom Sheldrake and two anonymous reviewers for their constructive and thoughtful reviews. Any use of trade, product, or firm names is for descriptive purposes only and does not imply endorsement by the U.S. Government.

REFERENCES CITED

Andersen, N.L., Jicha, B.R., Singer, B.S., and Hildreth, W., 2017, Incremental heating of Bishop Tuff sanidine reveals preeruptive radiogenic Ar and rapid remobilization from cold storage: Proceedings of the National Academy of Sciences, v. 114, p. 12,407–12,412, https://doi.org/10.1073/pnas.1709581114.

Bachmann, O., Dungan, M.A., and Lipman, P.W., 2000, Voluminous lava-like precursor to a major ash-flow tuff: Low-column pyroclastic eruption of the Pagosa Peak Dacite, San Juan volcanic field, Colorado: Journal of Volcanology and Geothermal Research, v. 98, p. 153–171, https://doi.org/10.1016/S0377-0273(99)00185-7.

Bachmann, O., Oberli, F., Dungan, M.A., Meier, M., Mundil, R., and Fischer, H., 2007, $^{40}Ar/^{39}Ar$ and U-Pb dating of the Fish Canyon magmatic system, San Juan Volcanic field, Colorado: Evidence for an extended crystallization history: Chemical Geology, v. 236, p. 134–166, https://doi.org/10.1016/j.chemgeo.2006.09.005.

Cebula, G.T., Kunk, M.J., Mehnert, H.H., Naeser, C.W., Obradovich, J.D., and Sutter, J.F., 1986, The Fish Canyon Tuff, a potential standard for the $^{40}Ar/^{39}Ar$ and fission-track methods: Terra Cognita, v. 6, p. 139–140.

Dalrymple, G.B., Alexander, E.C., Jr., Lanphere, M.A., and Kraker, G.P., 1981, Irradiation of samples for $^{40}Ar/^{39}Ar$ dating using the Geological Survey TRIGA reactor: U.S. Geological Survey Professional Paper 1176, 62 p., https://doi.org/10.3133/pp1176.

Druitt, T.H., et al., 2002, Episodes of cyclic Vulcanian explosive activity with fountain collapse at Soufriere Hills Volcano, Montserrat, *in*, Druitt, T.H., and Kokelaar, B.P., eds., The Eruption of Soufrière Hills Volcano, Montserrat, from 1995 to 1999: Geological Society of London Memoir 21, p. 281–306, https://doi.org/10.1144/GSL.MEM.2002.021.01.13.

Foreman-Mackey, D., Hogg, D.W., Lang, D., and Goodman, J., 2013, emcee: The MCMC hammer: Publications of the Astronomical Society of the Pacific, v. 125, p. 306–312, https://doi.org/10.1086/670067.

Hildreth, W., 2004, Volcanological perspectives on Long Valley, Mammoth Mountain, and Mono Craters: Several contiguous but discrete systems: Journal of Volcanology and Geothermal Research, v. 136, p. 169–198, https://doi.org/10.1016/j.jvolgeores.2004.05.019.

Jicha, B.R., Singer, B.S., and Sobol, P., 2016, Re-evaluation of the ages of $^{40}Ar/^{39}Ar$ sanidine standards and supereruptions in the western U.S. using a Noblesse multi-collector mass spectrometer: Chemical Geology, v. 431, p. 54–66, https://doi.org/10.1016/j.chemgeo.2016.03.024.

Kruschke, J.K., 2013, Bayesian estimation supersedes the *t* test: Journal of Experimental Psychology: General, v. 142, p. 573–603, https://doi.org/10.1037/a0029146.

Kuiper, K.F., Deino, A., Hilgen, F.J., Krijgsman, W., Renne, P.R., and Wijbrans, J.R., 2008, Synchronizing rock clocks of Earth history: Science, v. 320, p. 500–504, https://doi.org/10.1126/science.1154339.

Lee, J.-Y., Marti, K., Severinghaus, J.P., Kawamura, K., Yoo, H.-S., Lee, J.B., and Kim, J.S., 2006, A redetermination of the isotopic abundances of atmospheric Ar: Geochimica et Cosmochimica Acta, v. 70, p. 4507–4512, https://doi.org/10.1016/j.gca.2006.06.1563.

Lipman, P.W., 2006, Geologic map of the central San Juan caldera cluster, southwestern Colorado: U.S. Geological Survey Miscellaneous Investigations Map I-2799, 4 sheets, scale 1:50,000, with 34 p. text.

Lipman, P., Dungan, M., and Bachmann, O., 1997, Comagmatic granophyric granite in the Fish Canyon Tuff, Colorado: Implications for magma-chamber processes during a large ash-flow eruption: Geology, v. 25, p. 915–918, https://doi.org/10.1130/0091-7613(1997)025<0915:CGGITF>2.3.CO;2.

Mark, D.F., Renne, P.R., Dymock, R.C., Smith, V.C., Simon, J.I., Morgan, L.E., Staff, R.A., Ellis, B.S., and Pearce, N.J.G., 2017, High-precision $^{40}Ar/^{39}Ar$ dating of pleistocene tuffs and temporal anchoring of the Matuyama-Brunhes boundary, Quaternary Geochronology, v. 39, p. 1–23, https://doi.org/10.1016/j.quageo.2017.01.002.

Metz, J.M., and Mahood, G.A., 1985, Precursors to the Bishop Tuff eruption: Glass Mountain, Long Valley, California: Journal of Geophysical Research, v. 90, p. 11,121–11,126, https://doi.org/10.1029/JB090iB13p11121.

Min, K., Mundil, R., Renne, P.R., and Ludwig, K.R., 2000, A test for systematic errors in $^{40}Ar/^{39}Ar$ geochronology through comparison with U/Pb analysis of a 1.1-Ga rhyolite: Geochimica et Cosmochimica Acta, v. 64, p. 73–98, https://doi.org/10.1016/S0016-7037(99)00204-5.

Morgan, L.E., 2019, Argon geochronology data for La Garita caldera: U.S. Geological Survey data release, https://doi.org/10.5066/P9NACN2E.

Morgan, L.E., Mark, D.F., Imlach, J., Barfod, D., and Dymock, R., 2014, FCs-EK: A new sampling of the Fish Canyon Tuff $^{40}Ar/^{39}Ar$ neutron flux monitor, *in* Jourdan, F., et al., eds., Advances in $^{40}Ar/^{39}Ar$ Dating: From Archaeology to Planetary Sciences: Geological Society of London Special Publication 378, p. 63–67, https://doi.org/10.1144/SP378.21.

Phillips, D., and Matchan, E.L., 2013, Ultra-high precision $^{40}Ar/^{39}Ar$ ages for Fish Canyon Tuff and Alder Creek Rhyolite sanidine: New dating standards required?: Geochimica et Cosmochimica Acta, v. 121, p. 229–239, https://doi.org/10.1016/j.gca.2013.07.003.

Phillips, D., Matchan, E.L., Honda, M., and Kuiper, K.F., 2017, Astronomical calibration of $^{40}Ar/^{39}Ar$ reference minerals using high-precision, multi-collector (ARGUSVI) mass spectrometry: Geochimica et Cosmochimica Acta, v. 196, p. 351–369, https://doi.org/10.1016/j.gca.2016.09.027.

Renne, P.R., Swisher, C.C., Deino, A.L., Karner, D.B., Owens, T.L., and DePaolo, D.J., 1998, Intercalibration of standards, absolute ages and uncertainties in $^{40}Ar/^{39}Ar$ dating: Chemical Geology, v. 145, p. 117–152, https://doi.org/10.1016/S0009-2541(97)00159-9.

Renne, P.R., Mundil, R., Balco, G., Min, K., and Ludwig, K.R., 2010, Joint determination of ^{40}K decay constants and $^{40}Ar^*/^{40}K$ for the Fish Canyon sanidine standard, and improved accuracy for $^{40}Ar/^{39}Ar$ geochronology: Geochimica et Cosmochimica Acta, v. 74, p. 5349–5367, https://doi.org/10.1016/j.gca.2010.06.017.

Renne, P.R., Balco, G., Ludwig, K.R., Mundil, R., and Min, K., 2011, Response to the comment by W.H. Schwarz et al. on "Joint determination of ^{40}K decay constants and $^{40}Ar^*/^{40}K$ for the Fish Canyon sanidine standard, and improved accuracy for $^{40}Ar/^{39}Ar$ geochronology" by P.R. Renne et al. (2010): Geochimica et Cosmochimica Acta, v. 75, p. 5097–5100, https://doi.org/10.1016/j.gca.2011.06.021.

Renne, P.R., Mulcahy, S.R., Cassata, W.S., Morgan, L.E., Kelley, S.P., Hlusko, L.J., and Njau, J.K., 2012, Retention of inherited Ar by alkali feldspar xenocrysts in a magma: Kinetic constraints from Ba zoning profiles: Geochimica et Cosmochimica Acta, v. 93, p. 129–142, https://doi.org/10.1016/j.gca.2012.06.029.

Rutte, D., Pfänder, J.A., Koleška, M., Jonckheere, R., and Unterricker, S., 2015, Radial fast-neutron fluence gradients during rotating $^{40}Ar/^{39}Ar$ sample irradiation recorded with metallic fluence monitors and geological age standards: Geochemistry Geophysics Geosystems, v. 16, p. 336–345, https://doi.org/10.1002/2014GC005611.

Schwarz, W.H., and Trieloff, M., 2007, Intercalibration of ^{40}Ar-^{39}Ar age standards NL-25, HB3gr hornblende, GA1550, SB-3, HD-B1 biotite and BMus/2 muscovite: Chemical Geology, v. 242, p. 218–231, https://doi.org/10.1016/j.chemgeo.2007.03.016.

Simon, J.I., and Reid, M.R., 2005, The pace of rhyolite differentiation and storage in an "archetypical" silicic magma system, Long Valley, California: Earth and Planetary Science Letters, v. 235, p. 123–140, https://doi.org/10.1016/j.epsl.2005.03.013.

Vermeesch, P., 2018, IsoplotR: A free and open toolbox for geochronology: Geoscience Frontiers, v. 9, p. 1479–1493, https://doi.org/10.1016/j.gsf.2018.04.001.

Wotzlaw, J.-F., Schaltegger, U., Frick, D.A., Dungan, M.A., Gerdes, A., and Günther, D., 2013, Tracking the evolution of large-volume silicic magma reservoirs from assembly to supereruption: Geology, v. 41, p. 867–870, https://doi.org/10.1130/G34366.1.

Printed in USA